Intermediacy of Poly(L-proline) II and β-Strand Conformations in Poly(L-lysine) β-Sheet Formation Probed by Temperature-Jump/UV Resonance Raman Spectroscopy†

Renee D. JiJi,‡ Gurusamy Balakrishnan, Ying Hu,§ and Thomas G. Spiro*

Department of Chemistry, Princeton University, Princeton, New Jersey 08544

Received July 28, 2005; Revised Manuscript Received October 28, 2005

ABSTRACT: Ultraviolet resonance Raman spectroscopy (UVRR) in combination with a nanosecond temperature jump (T-jump) was used to investigate early steps in the temperature-induced α-helix to β-sheet conformational transition of poly(L-lysine) [poly(K)]. Excitation at 197 nm from a tunable frequency-quadrupled Ti:sapphire laser provided high-quality UVRR spectra, containing multiple conformation-sensitive amide bands. Although un-ionized poly(K) (pH 11.6) is mainly α-helical below 30 °C, there is a detectable fraction (∼15%) of unfolded polypeptide, which is mainly in the poly(L-proline) II (PPII) conformation. However, deviations from the expected amide I and II signals indicate an additional conformation, suggested to be β-strand. Above 30 °C un-ionized poly(K) forms a β-sheet at a rate (minutes) which increases with increasing temperature. A 22−44 °C T-jump is accompanied by prompt amide I and II difference signals suggested to arise from a rapid shift in the PPII/β-strand equilibrium. These signals are superimposed on a subsequently evolving difference spectrum which is characteristic of PPII, although the extent of conversion is low, ∼2% at the 3 μs time limit of the experiment. The rise time of the PPII signals is ∼250 ns, consistent with melting of short α-helical segments. A model is proposed in which the melted PPII segments interconvert with β-strand conformation, whose association through interstrand H-bonding nucleates the formation of β-sheet. The intrinsic propensity for β-strand formation could be a determinant of β-sheet induction time, with implications for the onset of amyloid diseases.

Several degenerative diseases, including Alzheimer's, Huntington's, Parkinson's, and transmissible spongiform encephalopathies (TSE), are associated with misfolding and aggregation of proteins (*1*). The misfolded proteins form fibrillous aggregates, termed amyloid fibrils, which have a cross-β-sheet structure in which the polypeptide backbone is perpendicular to the fibril axis (*2*). This allows the fibril to grow lengthwise with the addition of subsequent misfolded protein molecules. It is interesting to note that conditions which promote partial folding of proteins appear to promote fibril formation in vitro (*3*−*5*).

Certain proteins with abundant α-helical structure, including the prion protein (PrP^C) and apomyoglobin, convert to β-sheet-rich structures under denaturing conditions (*4*−*6*). What is equally provocative is the correlation between metastable α-helices and β-sheet amyloid formation. The β-amyloid (Aβ) peptide involved in Alzheimer's disease and its constituent fragments contain no stable secondary structure in aqueous solutions (*7*, *8*), but when the nascent helical structure is partially stabilized by low concentrations of TFE (20%), Aβ's aggregation rate is maximal (*3*). Other kinetic studies of Aβ oligomerization have reported the emergence of transient α-helical structure just prior to the appearance of β-strand structure (*9*), indicating that the α-helix to β-sheet transition is associated with aggregation. The physical mechanism of the α-helix → β-sheet transition is uncertain. It is enticing to speculate that an intermediate of this transition may be similar to the structure characterized in poly(L-proline), termed PPII, as its presence has been indicated in partially denatured proteins (*10*).

PPII has an extended 3_1-helical structure with three residues per turn ($\phi = -70°$, $\psi = +145°$), which minimizes interactions between side chains. In 1968, similarities in the circular dichroism (CD)[1] spectra of PPII and poly(L-glutamic acid) [poly(E)] led Tiffany and Krimm to propose that the unfolded conformation of poly(E) and poly(L-lysine) [poly(K)] contained significant amounts of PPII structure (*11*). Since then, PPII structure has been identified in numerous unfolded peptides by various spectroscopic methods. These proteins include the unstructured Aβ peptide fragment ($A\beta_{(1-28)}$, pH 4) (*7*), the full-length peptide and several N-terminal fragments ($A\beta_{(1-40)}$, $A\beta_{(1-9,16,28)}$, pH 7.4, 0 °C) (*12*), the reduced ovine PrP^{93-244} (pH 4.0), unfolded poly-

† This work was supported by NIH Grants R01 GM 025158 to T.G.S. and F32 AG 022770 to R.D.J.

* To whom correspondence should be addressed. Telephone: (609) 258-3907. Fax: (609) 258-0348. E-mail: spiro@princeton.edu.

‡ Current address: Department of Chemistry, University of Missouri−Columbia, Columbia, MO 65211.

§ Current address: Department of Food Science, Cornell University, Ithaca, NY 14853.

[1] Abbreviations: UVRR, ultraviolet resonance Raman; T-jump, temperature jump; CD, circular dichroism; poly(K), poly(L-lysine); PPII, poly(L-proline) II; poly(E), poly(L-glutamic acid); poly(A), poly(L-alanine).

10.1021/bi051507v CCC: $33.50
Published on Web 12/08/2005

(K) (*13*), ribonuclease A (*14*), and a seven-residue nonhelical alanine peptide (XAO) (*15*). Studies of short alanine peptides reveal that the unfolded conformation is primarily PPII structure (*15*−*18*). PPII structure has also been observed in prefibrillar intermediates of human lysozyme (*10*). It is becoming clear that partial unfolding of proteins promotes amyloid formation and that PPII structure is associated with unfolded proteins. However, whether PPII structure is the decisive intermediate in the α-helix to β-sheet conformational transition remains unclear.

While identifying the initial protein conformational changes that lead to protein misfolding is critical to understanding the events that lead to the eventual polymerization phenomena of amyloidogenic proteins, rapid oligomerization and aggregation make it difficult to study amyloidogenic proteins such as Aβ and PrP. An alternative approach is to use a model system such as poly(K). Because of its structural plasticity and ease of manipulation, poly(K) is a good candidate system for modeling the dynamics of the initial protein conformation changes involved in α-helix to β-sheet transitions. At high pH, poly(K) is α-helical and readily converts to β-sheet structure at elevated temperatures (*19*).

The major protein conformations, α-helix and β-sheet, can be distinguished by their UVRR spectra (*20*−*22*). The protein conformational sensitivity of UVRR arises from the selective excitation of the $\pi^* \leftarrow \pi$ electronic transition of the amide bonds. The excitation maximum for the $\pi^*_3 \leftarrow \pi_2$ dipole-allowed transition is 188 nm. Although amide modes are readily detected below 220 nm, enhancement increases rapidly at shorter wavelengths. Our laboratory has exploited the capabilities of a frequency-quadrupled Ti:sapphire laser (*23*) to achieve high-quality amide spectra via excitation at 197 nm.

Using both steady-state and time-resolved temperature-jump (T-jump) ultraviolet resonance Raman (UVRR) spectroscopy, the early kinetic intermediates in the α-helix to β-sheet pathway of poly(K) have been investigated. Steady-state UVRR spectra at 197 nm excitation reveal that poly(K) exists in a complex equilibrium of conformations. This equilibrium is markedly shifted toward PPII at low pH, while high pH promotes a mixture of α-helical and PPII structure. T-jump difference spectra reveal that the initial events in the α-helix to β-sheet conformation change involve unfolding of a small fraction of α-helical structure. Further, the unfolded conformation of poly(K) at early times appears to contain a fraction of β-strand structure.

EXPERIMENTAL PROCEDURES

Materials. Poly(L-lysine) hydrochloride (MW 22100) was obtained from Sigma Aldrich (St. Louis, MO) and used without further purification. Samples were prepared by dissolution in doubly deionized water, and the pH was adjusted to 4.0 (unfolded) or 11.6 (α-helical) using 3 M hydrochloric acid and 4 M sodium hydroxide. β-Sheet poly(K) [β-poly(K)] was generated by heating a solution of the peptide, at pH 11.6, to 55 °C for 15 min. For experiments in 40% TFE (trifluoroethanol) and 60% glycerol, poly(K) was dissolved in doubly deionized water, and the pH was adjusted to 12.0 prior to addition of the appropriate volume of organic solvent. The concentration of the peptide was 2−3 mg/mL for UVRR studies.

Circular Dichroism (CD). CD data were collected over the wavelength range of 190−250 nm, with 1 nm spectral resolution, and averaged for 5 s at each wavelength. The concentration of the peptide was 0.5 mg/mL at pH 11.6 with 50 mM sodium perchlorate. Sodium perchlorate was added to maintain similar solution conditions between the UVRR and CD studies. CD spectra were collected on an Aviv 62DS CD spectrometer.

Ultraviolet Resonance Raman (UVRR). UVRR spectra were measured using the fourth harmonic from a tunable (193−210 nm) 1 kHz frequency quadrupled Ti:sapphire laser (Photonics Industries, Bohemia, NY) (*23*). The Ti:sapphire laser was pumped using the second harmonic of a Nd:YLF laser (Photonics Industries, Bohemia, NY). All samples were excited at 197 nm, the pulse width was ∼25 ns, and the average power at the sample was less than 1 mW. Scattered light was collected in the 135° backscattering geometry and dispersed using a 1.26 m spectrograph (Spex 1269) equipped with a 3600 groove/mm holographic grating. An intensified photodiode array detector (Roper Scientific) was used for detection of the scattered light. Win Spec software (Roper Scientific) was used for data collection. The experimental apparatus is described in detail elsewhere (*24*). Spectra were calibrated using a standard cyclohexane spectrum, and 50 mM perchlorate (ClO_4^-) was used as an internal intensity standard in all samples.

Temperature Jump (T-Jump). A Q-switched Nd:YLF laser was used to pump a tunable (1.8−2.05 μM) KTA-crystal-based OPO (Phontonics Industries, Bohemia, NY) to generate ∼10 ns laser pulses at 1.9 μm [see Balakrishnan et al. for a detailed description (*24*)]. The 0.8−1.2 mJ 1.9 μm IR pulses were used to generate a rapid 22−23 °C T-jump. Excitation of the sample at 1.9 μm (absorbance maximum of water) leads to a rapid (<70 ps) T-jump of the solvent water (*25*). The initial temperature was held between 21 and 22 °C, resulting in a final temperature range of 43−45 °C.

The change in temperature was measured using the O−H stretching band of water at 3400 cm^{-1}, which is red shifted at higher temperatures (*26*). A calibration curve was constructed for 197 nm excitation and used to determine the T-jump of the solution upon excitation (*24*).

Sampling Systems. For steady-state UVRR experiments, a peristaltic pump (Cole Palmer Instrument Co., Vernon Hills, IL) was used to circulate ∼4 mL of sample solution through at 24 gauge needle tip (Hamilton Co., Reno, NV). A water-jacketed sample reservoir, of in-house design, was used to maintain and control the solution temperature. The exiting solution was guided by two metal wires (0.015 diameter), separated by less than 1 mm, creating a narrow thin film which was excited by the 197 nm laser light. A stream of N_2 was passed over the sample to remove ambient O_2.

Given that the α-helix to β-sheet conformational transition is not rapidly reversible, a single pass flow system was used for the T-jump experiments. Two water-jacketed 50 mL glass syringes (BD, Franklin Lakes, NJ) were used as a sample reservoir and a rapid cooling sink. The reservoir was maintained at 21−22 °C, and the sink was held at less than 10 °C. A Harvard apparatus infusion/withdrawal syringe pump (model no. 915) was used to pump the solution through the wire-guided sampling system and withdraw the sample back into the cooling sink after heating. The total volume

of sample used for these experiments was 350 mL at 2−3 mg/mL. The 50 mL aliquots were rapidly cooled (<1 min) in the sink syringe to prevent β-sheet formation. The solution was allowed to rest for at least 15−30 min before reexposure to the T-jump. No detectable differences in the UVRR spectra of the sample were observed due to repeated exposure to the T-jump. However, the 50 mL aliquots were limited to three to four sampling intervals.

Data Analysis. All spectra were calibrated using Grams AI (Thermo Electron Corp., formerly Galactic Industries). The data were analyzed using either the Grams AI or Matlab (Mathworks, Natick, MA) platforms.

RESULTS

Assignment of the Major Spectral Features in the UVRR Spectra of the Three Conformers of Poly(K). There are three structurally sensitive regions in the UVRR spectra of peptides and proteins, the amide I (1600−1690 cm^{-1}), amide II (1450−1580 cm^{-1}), and amide III/S (1200−1420 cm^{-1}) regions. The amide I mode is composed mainly of carbonyl C═O stretching, and its frequency is sensitive to hydrogen bonding and interresidue coupling (*27*, *28*). The amide II mode is composed mainly of an out-of-phase combination of N−H in-plane bending (NH ib) and C−N stretching (CN s) and is sensitive to the relative contribution of NH ib (*29*). The amide III mode is an in-phase combination of NH ib and CN s (*30*). The structural sensitivity of the amide III and S modes arises from the mechanical coupling of the NH ib and (C)C_α−H bending (C_αH b) coordinates (*30*). This coupling is the likely source of the observational relationship between the amide III frequency and the ψ dihedral angle (*31*). Structural assignments are based on the systematic studies of Krimm and co-workers (*29*, *32*−*35*), which provide detailed comparisons between normal-mode calculations and observed frequencies of the structural conformers of crystalline homopolypeptides, including poly(L-alanine) [poly(A)] and poly(L-glycine) [poly(G)].

As a prelude to exploring the fast kinetics of the α-helix to β-sheet conformation change, UVRR spectra were collected for a series of conditions known to promote α-helical (high pH), β-sheet (high pH, high temperature), and unfolded (low pH) conformations of poly(K). These new spectra (Figure 1) are highly resolved and show multiple components, which indicate a degree of structural heterogeneity in the solutions. Understanding these basis spectra is essential to discerning the complex shifts in equilibrium structure associated with the α-helix to β-sheet conformational transition.

β-Sheet. At 50 °C, α-poly(K) rapidly (∼2 min) converts to a β-sheet-structured peptide (*36*). The UVRR spectrum of this solution (Figure 1, top) shows a single amide I band (1670 cm^{-1}), but the amide II band is broad and asymmetrical (Figure 1), consistent with the observation of both low- and high-frequency components in crystalline β-sheet poly(L-alanine) [β-poly(A)] (*29*). The amide III and S maxima of β-poly(K) occur at 1237 and 1406 cm^{-1}, respectively, consistent with previous observations (*37*, *38*). Several less intense contributions are better resolved in the second derivative spectrum of β-poly(K) (Figure 1). There is a moderately strong band at 1354 cm^{-1}, which is tentatively assigned as an amide S mode in accordance with previously observed Raman bands for β-poly(A) (*29*). All of these observations are consistent with previous UVRR studies (*22*, *30*). The β-sheet structural assignments of the UVRR amide modes are summarized in Table 1, along with the α-helix and unfolded structural assignments (discussed below).

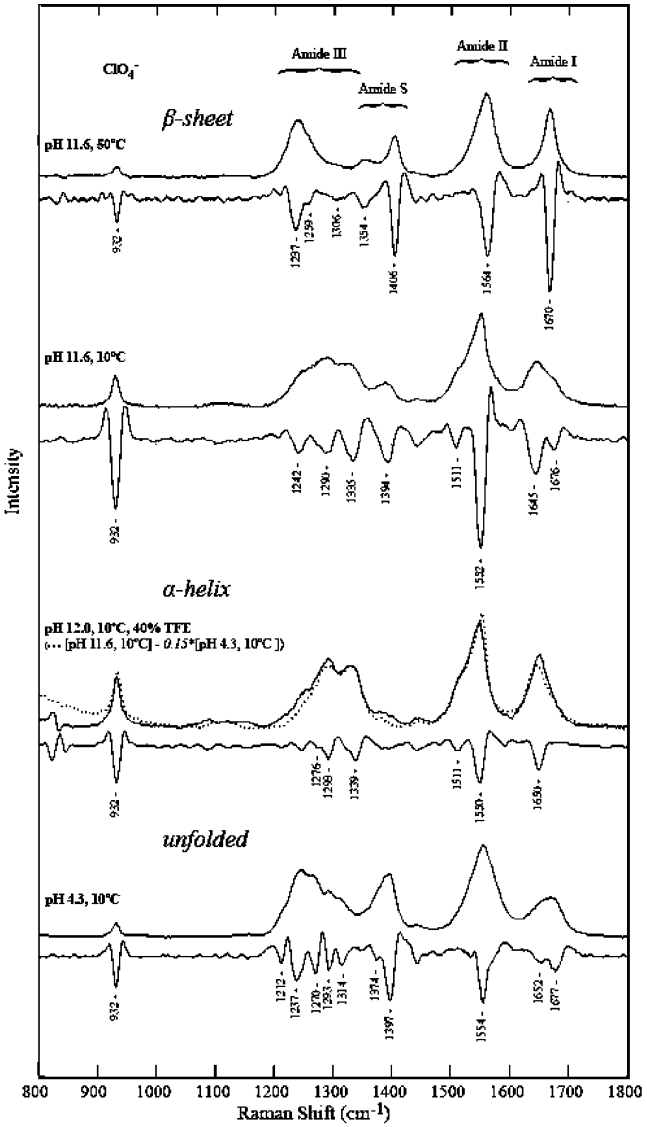

FIGURE 1: UVRR (top) and second derivative (bottom) spectra of poly(K) under the indicated solution conditions. The dotted line in the third panel is the second spectrum minus the bottom spectrum with a 15% weighting.

Table 1: Assignment of the UVRR Amide Modes of Poly(K)

	shift (cm^{-1})		
	α-helical	β-sheet	unfolded (PPII)
amide I		1670	1677
	1650		1652
amide II	1550	1564	1554
	1511		
amide S		1406	1397
		1354	1374
amide III	1339	1306	1314
	1293		1293
	1276	1259	1270
		1237	1237
			1212

α-Helix. Although un-ionized poly(K) is mainly α-helical at low temperature, the UVRR spectrum at pH 11.6 at 10

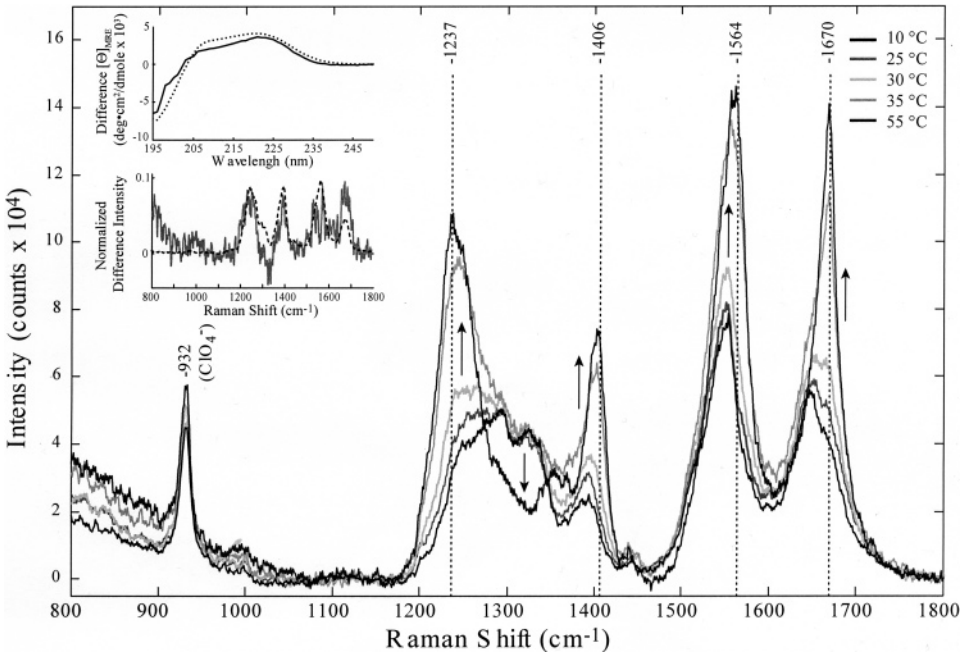

FIGURE 2: Temperature-dependent UVRR spectra of poly(K) at pH 11.6. Arrows indicate the direction of the intensity change upon going from 10 to 55 °C. Inset: Temperature difference spectra (—) for poly(K) at pH 11.6 via CD (top, 20−4 °C) and via UVRR (bottom, 20−5 °C), and pH 11.6−4.3 difference spectra (- - -) at low temperature [10 °C, pH 4.3, and 4 °C (CD) or 5 °C (UVRR)] with 10% weighting (i.e., 10% unfolding).

°C reveals a significant fraction of unfolded peptide, as can be seen by the effect of adding 40% trifluoroethanol (TFE), which is known to stabilize α-helices (*39*−*41*). Bands at 1676, 1394, and 1242 cm^{-1}, which are attributed to the unfolded peptide (see below), are nearly eliminated. The 40% TFE spectrum can be closely matched (Figure 1, dotted line) by subtracting the pH 4.3 spectrum of unfolded protein (bottom) from the pH 11.6 spectrum, with a 0.15 weighting factor. The 40% TFE spectrum shows the main amide I, II, and III frequencies at canonical α-helix frequencies 1650, 1550, and 1276/1293/1339 cm^{-1}. A second amide II component is evident as a prominent shoulder at 1511 cm^{-1} and is assigned to the A component, computed at 1519 cm^{-1} in α-poly(A) (*29*), while the main 1550 cm^{-1} band is assigned to the two E symmetry components.

The α-helical amide band is shifted up 5 cm^{-1} (1645 → 1650 cm^{-1}) in 40% TFE, reflecting the dehydrating effect of the organic solvent (a less effective dehydrating medium, 60% glycerol, produced a 2 cm^{-1} upshift; data not shown). The amide I band is sensitive to the extent of solvent hydrogen bonding with the backbone carbonyl. The IR amide I′ band of α-poly(K) is even lower, 1638 cm^{-1}(*42*), the position expected for the fully hydrated α-helix in D_2O. The IR/Raman frequency difference reflects the characteristic downshift of the amide I frequency upon N-deuteration (*43*).

Unfolded. At acidic pH the lysine side chains are protonated, and poly(K) is fully unfolded. Our 197 nm UVRR spectrum (Figure 1, bottom) is similar to the 206 nm UVRR spectrum published recently by Mikhonin et al. (*44*) and can be similarly assigned to PPII (Table 1) on the basis of frequency matches to XAO (*17*), a short polypeptide which has been established via NMR to be mainly in the PPII conformation (*15*). However, the bands are broad, probably reflecting a distribution of conformations, consistent with the early CD analysis by Tiffany and Krimm (*45*). The breadth and asymmetry of the amide I band also reflect interresidue coupling of the C═O oscillators (*46*).

We note that the band at 1270 cm^{-1} is proposed by Mikhonin et al. (*44*) to arise from an β-strand structure, but this assignment seems unlikely since its temperature dependence parallels that of the neighboring 1237 cm^{-1} PPII band (*44*), whereas the two should have exchanged intensity if there are interconverting structures. More likely the 1270 cm^{-1} band is an additional PPII amide III component, although its relative intensity is lower in the UVRR spectra of XAO and other alanine peptides (*17*, *44*).

Steady-State Temperature Profile of the α-Helix to β-Sheet Conformational Transition. UVRR spectra were collected at 5 °C intervals from 10 to 55 °C at pH 11.6 and a concentration of 2−3 mg/mL (Figure 2). Although previous studies have indicated a sharp two-state transition from α-helix to β-sheet (*38*, *47*, *48*), the absence of isosbestic points in the UVRR spectra (Figure 2) signals at least one additional component. The higher concentrations employed in the previous studies may explain the failure to detect intermediates, since the intermolecular association involved in β-sheet formation is highly concentration dependent. We note that McColl et al. (*13*) did detect Raman optical activity (ROA) signals (albeit associated with side chain conformation) which were different from the limiting α-helix and β-sheet signals.

As noted above, the low-temperature UVRR spectra reveal a fraction of unfolded molecules, as well as the dominant α-helix structure. This fraction increases with increasing temperature, up to about 30 °C; the intensity of the amide I, II, III, and S bands increased gradually with increasing temperature (Figure 2). A least-squares fit of the CD difference spectrum of α-poly(K) at pH 11.6 between 4 and 20 °C indicates that ∼10% of the helical structure is lost in this range to an unfolded conformation like that at low pH,

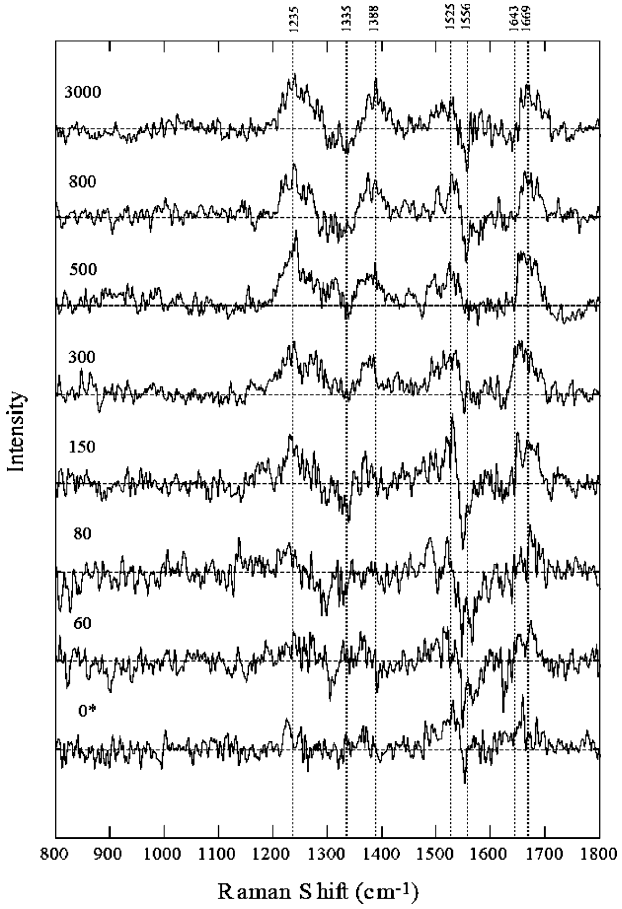

FIGURE 3: UVRR T-jump (22−44 °C) difference spectra of poly(K) (pH 11.6) at the indicated delay times (ns) (left side, above spectrum). The asterisk indicates overlapping pump and probe pulses; the limit of the time resolution is ∼40 ns.

PPII. Both the CD and UVRR temperature difference spectra up to 30 °C can be reproduced fairly closely by a combination of the unfolded (pH 4.3, 4 °C) and α-helical (pH 11.6, 4 °C) spectra (Figure 2, inset). However, the UVRR difference spectrum deviates from the modeled spectrum in the amide I and II regions; we interpret this as reflecting a contribution from *β*-strand structure, as discussed below.

Above 30 °C, the spectra change rapidly toward the *β*-sheet spectrum, indicating an initiation temperature, T_β, around 30 °C. Above 35 °C, the scattering intensity progressively increased at frequencies consistent with the formation of *β*-sheet structure, accounting for the second phase of conformational change. In addition, a small decrease in spectral intensity was observed between 1270 and 1330 cm^{-1} in the amide III region, indicating loss of α-helical structure [cross sections are much lower for α-helix than *β*-sheet (*49*)].

Nanosecond T-Jump Studies of the α-Helix to β-Sheet Conformational Transition. A nanosecond T-jump was employed to monitor events prior to the α-helix to *β*-sheet conformational transition of poly(K), which occurs on the minutes time scale. UVRR spectra were collected at time delays from 0 to 3 *μ*s, following excitation of the solvent water by a 1.9 *μ*m IR laser pulse, which produced a 22−44 °C jump. The difference spectra (pump plus probe minus probe only) are shown in Figure 3. They show a clear evolution on the ∼100 ns time scale toward a spectrum with weak negative features at ∼1335 and 1643 cm^{-1}, the α-helix amide III and I positions, and strong positive features at

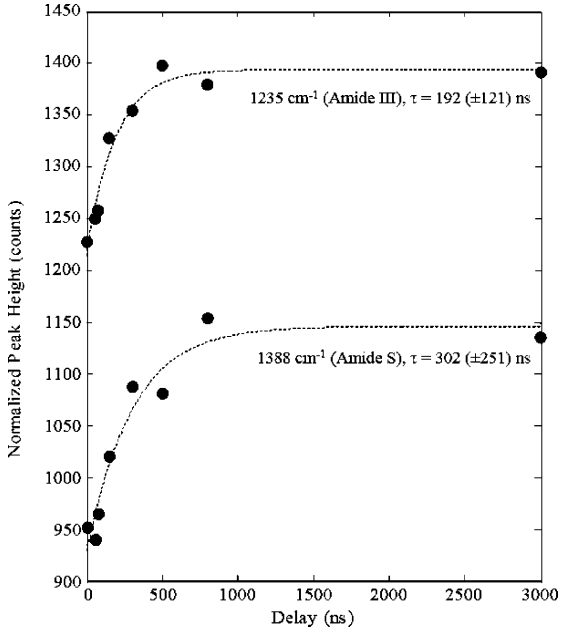

FIGURE 4: Exponential fits to the normalized peak intensities of the amide III band at 1242 cm^{-1} and the amide S band at 1394 cm^{-1}. Data were normalized to the probe only amide III band at 1242 cm^{-1}.

∼1235, ∼1388, and ∼1669 cm^{-1}, positions characteristic of the PPII amide III, S, and I bands. When the 1235 and 1388 cm^{-1} were plotted against time, the data could be fit to single exponential delays with time constants of 192 (±121) ns and 302 (±251) ns (Figure 4), respectively, similar to time constants reported for the melting of short α-helices (*50*, *51*). However, the limiting amplitudes of these bands are only about 2% of those produced by unfolded PLL at low pH (Figure 2). (This is why the T-jump difference spectra are quite noisy). Thus the data implicate rapid unfolding of only a small fraction of the α-helix structure present at 22 °C.

Although the T-jump difference spectra resemble the expected signals for α-helix melting to PPII, there are significant differences at the amide I and especially at the amide II positions. Compared to the spectrum obtained by subtracting low-temperature pH 11.6 (mostly α-helix) and 4.3 (mostly PPII) spectra (Figure 5), the T-jump difference amide I band is stronger than expected, relative to amide III and S, while amide II is weaker than expected and is shifted to lower frequency, as indicated by the sigmoidal signal. These deviations are similar to, but more pronounced than, those noted (above) for the static 20−4 °C temperature difference spectrum at pH 11.6 (Figure 5). Moreover, evolution of the positive amide I and sigmoidal amide II signals precedes that of the PPII amide III and S bands in the T-jump difference spectrum. They can even be seen in the zero-time spectrum, arising within the ∼40 ns time resolution of the instrument (convolution of pump and probe pulse widths).

Thus, in addition to the α-helix → PPII transition, we detect prompt formation of an additional conformation, having enhanced amide I and diminished amide II intensity, as well as a downshifted position for amide II. Some of this additional conformation, which we suggest to be *β*-strand, is also formed at equilibrium, at temperatures below the *β*-sheet initiation temperature.

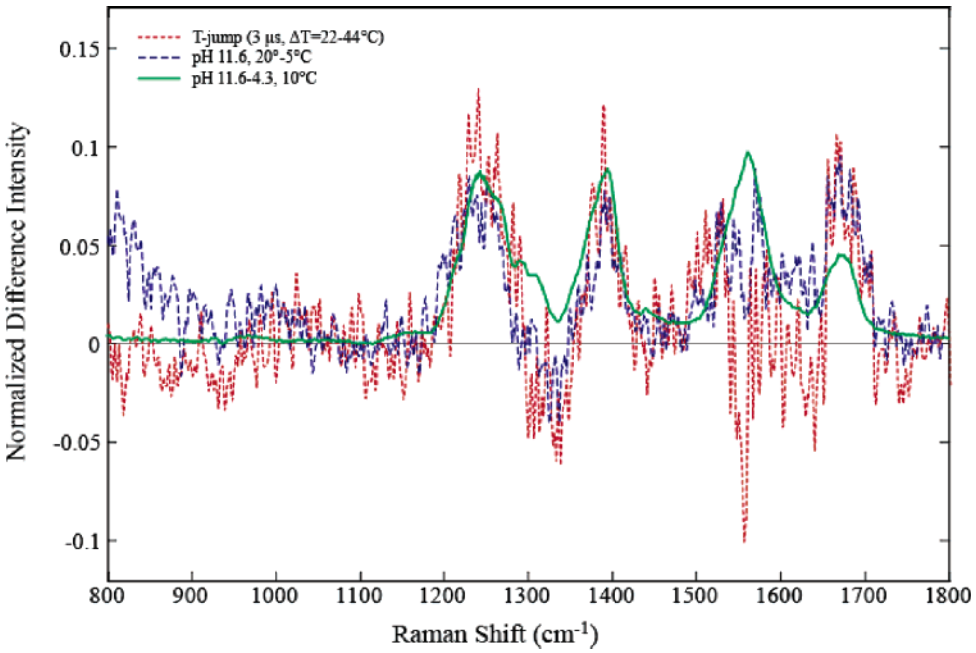

FIGURE 5: Comparison of difference UVRR spectra for a 22−44 °C T-jump (pH 11.6) at 3 μs (···), the static 20−5 °C temperature difference at pH 11.6 (- - -), and the pH 11.6−4.3 difference at 10 °C (—). The spectra were scaled to the same amplitude at the 1235 (amide III) and 1388 (amide S) cm^{-1} peaks.

DISCUSSION

Poly(K) was chosen as a model system for fast kinetic study because of its facile conversion from α-helix to β-sheet upon heating. We wanted to establish the steps in this process and to investigate the nature of intermediate conformations via UVRR spectroscopy. β-Sheet formation involves interas well as intramolecular H-bond formation between adjacent strands and is concentration-dependent. At the dilute concentrations employed in this study, sheet formation by poly(K) takes minutes and is clearly separated kinetically from the nanosecond to microsecond time scale of the T-jump experiments.

The β-sheet fibrils associated with amyloid diseases generally form from unfolded proteins which had been considered to be disordered but have been shown to contain significant PPII content (*52*), and PPII has therefore been suggested to be the "killer conformation" in the development of neurodegenerative disease (*52*). However, the mechanism whereby PPII could be responsible for β-sheet formation has not been addressed.

The present data establish that, although polylysine is mainly α-helical at high pH and low temperature, a detectable fraction, on the order of 15%, is unfolded and has PPII-like amide III and S bands. These same PPII-like bands are apparent in the T-jump difference spectrum, and the time constant for their appearance, ∼250 ns, is similar to those reported for the melting of short poly(A) helices. This similarity suggests that the poly(K) helices melt in short segments. Moreover, the extent of α-helix → PPII conversion is low, although at the final T-jump temperature, 44 °C, essentially all of the poly(K) eventually forms β-sheet. At the 3 μs time limit of the T-jump experiment, the PPII intensities correspond to about 2% of that expected [from the poly(K) spectrum at low pH] if all of the molecules adopted this conformation. Thus the poly(K) α-helix is intrinsically quite stable; its transformation to β-sheet is driven by the greater stability conferred by the interstrand H-bonds. If the PPII conformation is on the pathway to sheet formation, it is a low-concentration intermediate.

The T-jump spectra establish the formation of an additional conformer, via the amide I and II signals. Positive amide I and sigmoidal amide II signals appear in the T-jump difference spectrum within the ∼40 ns time resolution of the experiment, and these signals are later superimposed on the evolving PPII amide III and S signals. Consequently, the 3 μs difference spectrum deviates at the amide I and II positions from that expected from the α-helix → PPII conversion. Similar deviations are seen in the equilibrium melting spectra, although to a lesser extent.

Structural interpretation of these new signals is uncertain, but we offer the suggestion that they arise from conversion of PPII to β-strand conformation. Since the signals arise promptly, they do not reflect α-helix melting, which occurs on the 100 ns time scale. However, PPII could convert rapidly to another conformation, since no intrastrand H-bonds need be broken. We are unable to model the spectrum of an individual β-strand, since β-strands are unstable with respect to association via interstrand H-bonds. However, Abe and Krimm (*33*) concluded from their vibrational analysis of crystalline polymorphs of poly(G) that amide II does shift to low values for extended peptide structures, such as β-strand. A downshift relative to β-sheet would be expected from the loss of interstrand H-bonds (and their replacement by weaker H-bonds from water), since amide II frequency is known (*53*) to correlate directly with H-bond strength. Thus the downshifted amide II position seen in the sigmoidal difference signal would be a plausible correlate of β-strand formation.

The appealing aspect of the postulated β-strand population is that it is properly aligned for the formation of β-sheet interstrand H-bonds. We propose a model for β-sheet formation (Figure 6) in which α-helical segments of poly(K) melt transiently to segments of extended conformation,

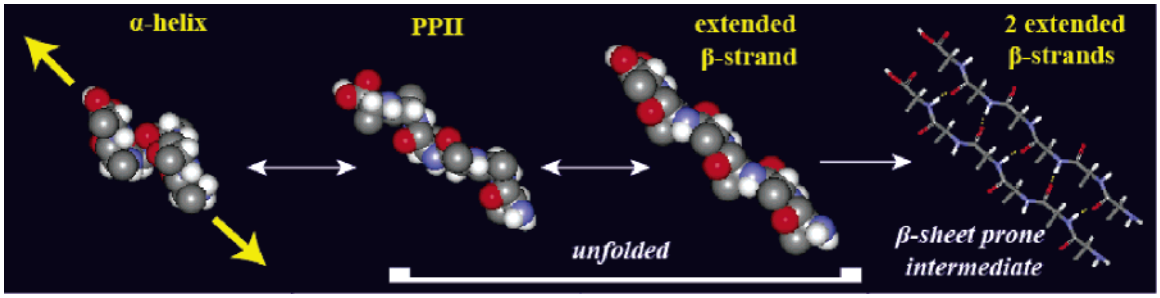

FIGURE 6: A model of the structural equilibrium between the α-helix, PPII, and β-strand and the penultimate step in β-sheet formation, formation of hydrogen bonds between two β-strands (shown as yellow dotted lines).

replacing the α-helix intrastrand H-bonds with water H-bonds. However, the melted segments are suggested to be in rapid equilibrium between PPII and β-strand conformations. PPII is dominant, but the β-strand fraction increases with increasing temperature; consequently, additional β-strand is formed following a T-jump. A prompt β-strand signal is observed because there is preexisting PPII structure at the initial temperature (22 °C), which converts rapidly during the T-jump, prior to the α-helix melting.

Connecting the β-strand segments with interstrand H-bonds would then be the rate-determining step in β-sheet formation. A critical number of these interstrand links would be required for nucleation of β-sheet structure. Thus the β-sheet induction time would depend sensitively on the β-strand population, which increases with increasing temperature. Consistent with this model is the observation that alanine polypeptides which are longer than 10 residues also form β-sheet structures at high temperatures, but this process takes many hours (*54*), whereas β-sheet formation takes only minutes for poly(K). The UVRR spectra of melted poly(A) helices show PPII character, with no evidence of the anomalous amide I and II signals seen for poly(K) (*26*). Likewise, the T-jump difference spectra do not show these additional signals (*26*). Thus the additional conformation, which we postulate to be β-strand, is much lower for poly(A) than for poly(K), and the β-sheet induction time is correspondingly much longer.

CONCLUSIONS

α-Helical poly(K) is shown to undergo thermal melting prior to β-sheet formation. The UVRR spectra show that the thermally unfolded helix is a mixture of PPII and another conformation, suggested to be β-strand. The putative β-strand signals are also observed in T-jump difference UVRR spectra. They are generated within the ~40 ns instrument resolution, suggesting a prompt shift of an equilibrium involving preexisting PPII segments. These signals are superimposed on the more slowly evolving helix melting spectrum, consisting of additional PPII signals. Helix melting for poly(K) is on the same time scale, ~250 ns, as has been reported for melting of short poly(A) helices, but the extent of conversion to PPII structure is only ~2%.

A model for β-sheet formation is proposed, in which short segments of poly(K) helices melt to PPII conformations, which equilibrate rapidly with β-strand conformation. The equilibrium shifts toward β-strand with increasing temperature. β-Sheet then nucleates via H-bonding between β-strands, the induction time depending sensitively on the β-strand population. The much longer induction time for poly(A) (hours) than poly(K) (minutes) may be due to a much lower β-strand population; reported UVRR spectra of alanine polypeptides do not contain the putative β-strand signals observed for poly(K).

It may generally be the case that the rate of β-sheet formation depends on the propensity for forming the β-strand conformation. This hypothesis could have important implications for the onset of amyloid diseases.

ACKNOWLEDGMENT

The authors thank Prof. Janette Carey for help with the CD measurements.

REFERENCES

1. Dobson, C. M. (2001) The structural basis of protein folding and its links with human disease, *Philos. Trans. R. Soc. London, Ser. B: Biol. Sci. 356*, 133−145.
2. Tycko, R. (2004) Progress towards a molecular-level structural understanding of amyloid fibrils, *Curr. Opin. Struct. Biol. 14*, 96−103.
3. Fezoui, Y., and Teplow, D. B. (2002) Kinetic studies of amyloid β-protein fibril assembly−Differential effects of α-helix stabilization, *J. Biol. Chem. 277*, 36948−36954.
4. Morillas, M., Vanik, D. L., and Surewicz, W. K. (2001) On the mechanism of α-helix to β-sheet transition in the recombinant prion protein, *Biochemistry 40*, 6982−6987.
5. Fandrich, M., Fletcher, M. A., and Dobson, C. M. (2001) Amyloid fibrils from muscle myoglobin, *Nature 410*, 165−166.
6. Fandrich, M., Forge, V., Buder, K., Kittler, M., Dobson, C. M., and Diekmann, S. (2003) Myoglobin forms amyloid fibrils by association of unfolded polypeptide segments, *Proc. Natl. Acad. Sci. U.S.A. 100*, 15463−15468.
7. Eker, F., Griebenow, K., and Schweitzer-Stenner, R. (2004) A$\beta_{(1-28)}$ fragment of the amyloid peptide predominantly adopts a polyproline II conformation in an acidic solution, *Biochemistry 43*, 6893−6898.
8. Lee, J. P., Stimson, E. R., Ghilardi, J. R., Mantyh, P. W., Lu, Y. A., Felix, A. M., Llanos, W., Behbin, A., Cummings, M., Vancriekinge, M., Timms, W., and Maggio, J. E. (1995) ^{1}H NMR of Aβ amyloid peptide congeners in water solution. Conformational-changes correlate with plaque competence, *Biochemistry 34*, 5191−5200.
9. Kirkitadze, M. D., Condron, M. M., and Teplow, D. B. (2001) Identification and characterization of key kinetic intermediates in amyloid β-protein fibrillogenesis, *J. Mol. Biol. 312*, 1103−1119.
10. Blanch, E. W., Morozova-Roche, L. A., Cochran, D. A. E., Doig, A. J., Hecht, L., and Barron, L. D. (2000) Is polyproline II helix the killer conformation? A Raman optical activity study of the amyloidogenic prefibrillar intermediate of human lysozyme, *J. Mol. Biol. 301*, 553−563.
11. Tiffany, M. L., and Krimm, S. (1968) New chain conformations of poly(glutamic acid) and polylysine, *Biopolymers 6*, 1379−1382.
12. Danielsson, J., Jarvet, J., Damberg, P., and Graslund, A. (2005) The Alzheimer β-peptide shows temperature-dependent transitions between left-handed 31-helix, β-strand and random coil secondary structures, *FEBS J. 272*, 3938−3949.
13. McColl, L. H., Blanch, E. W., Gill, A. C., Rhie, A. G. O., Ritchie, M. A., Hecht, L., Nielsen, K., and Barron, L. D. (2003) A new perspective on β-sheet structures using vibrational Raman optical

activity: From poly(L-lysine) to the prion protein, *J. Am. Chem. Soc. 125*, 10019−10026.
14. Wilson, G., Hecht, L., and Barron, L. D. (1996) Residual structure in unfolded proteins revealed by Raman optical activity, *Biochemistry 35*, 12518−12525.
15. Shi, Z., Olson, C. A., Rose, G. D., Baldwin, R. L., and Kallenbach, N. R. (2002) Polyproline II structure in a sequence of seven alanine residues, *Proc. Natl. Acad. Sci. U.S.A. 99*, 9190−9195.
16. Eker, F., Griebenow, K., Cao, X., Nafie, L. A., and Schweitzer-Stenner, R. (2004) Preferred peptide backbone conformations in the unfolded state revealed by the structure analysis of alanine-based (AXA) tripeptides in aqueous solution, *Proc. Natl. Acad. Sci. U.S.A. 101*, 10054−10059.
17. Asher, S. A., Mikhonin, A. V., and Bykov, S. (2004) UV Raman demonstrates that α-helical polyalanine peptides melt to polyproline II conformations, *J. Am. Chem. Soc. 126*, 8433−8440.
18. McColl, I. H., Blanch, E. W., Hecht, L., Kallenbach, N. R., and Barron, L. D. (2004) Vibrational Raman optical activity characterization of poly(L-proline) II helix in alanine oligopeptides, *J. Am. Chem. Soc. 126*, 5076−5077.
19. Davidson, B., and Fasman, G. D. (1967) Conformational transitions of uncharged poly-L-lysine. α-Helix-random coil-β structure, *Biochemistry 6*, 1616−1629.
20. Chi, Z., Chen, X. G., Holtz, J. S. W., and Asher, S. A. (1998) UV resonance Raman: Selective amide vibrational enhancement: Quantitative methodology for determining protein secondary structure, *Biochemistry 37*, 2854−2864.
21. Wang, Y., Purrello, R., and Spiro, T. G. (1989) UV photoisomerization of *N*-methylacetamide and resonance Raman enhancement of a new conformation: sensitive amide mode, *J. Am. Chem. Soc. 111*, 8274−8276.
22. Song, S. H., and Asher, S. A. (1989) UV resonance Raman studies of peptide conformation in poly(L-lysine), poly(L-glutamic acid), and model complexes: the basis for protein secondary structure determinations, *J. Am. Chem. Soc. 111*, 4295−4305.
23. Balakrishnan, G., Hu, Y., Nielsen, S. B., and Spiro, T. G. (2005) Tunable kHz deep ultraviolet (193−210 nm) laser for Raman applications, *Appl. Spectrosc. 59*, 776−781.
24. Balakrishnan, G., Hu, Y., and Spiro, T. G. (2005) (manuscript in preparation).
25. Phillips, C. M., Mizutani, Y., and Hochstrasser, R. M. (1995) Ultrafast thermally induced unfolding of RNAse-A, *Proc. Natl. Acad. Sci. U.S.A. 92*, 7292−7296.
26. Lednev, I. K., Karnoup, A. S., Sparrow, M. C., and Asher, S. A. (1999) α-Helix peptide folding and unfolding activation barriers: A nanosecond UV resonance Raman study, *J. Am. Chem. Soc. 121*, 8074−8086.
27. Wang, Y., Purrello, R., Georgiou, S., and Spiro, T. G. (1991) UVRR spectroscopy of the peptide-bond. 2. Carbonyl H-bond effects on the ground-state and excited-state structures of *N*-methylacetamide, *J. Am. Chem. Soc. 113*, 6368−6377.
28. Austin, J. C., Jordan, T., and Spiro, T. G. (1993) Ultraviolet resonance Raman studies of proteins and related model compounds, in *Biomolecular Spectroscopy* (Clark, R. J. H., and Hester, R. E., Eds.) pp 55−127, Wiley & Sons Ltd., New York.
29. Krimm, S., and Bandekar, J. (1986) Vibrational spectroscopy and conformation of peptides, polypeptides and proteins, in *Advances in Protein Chemistry* (Anfinson, C. B., Edsall, J. T., and Richards, F. M., Eds.) pp 181−365, Academic Press, New York.
30. Wang, Y., Purrello, R., Jordan, T., and Spiro, T. G. (1991) UVRR spectroscopy of the peptide-bond. 1. Amide-S, a nonhelical structure marker, is a $C_\alpha H$ bending mode, *J. Am. Chem. Soc. 113*, 6359−6368.
31. Asher, S. A., Ianoul, A., Mix, G., Boyden, M. N., Karnoup, A., Diem, M., and Schweitzer-Stenner, R. (2001) Dihedral ψ angle dependence of the amide III vibration: A uniquely sensitive UV resonance Raman secondary structural probe, *J. Am. Chem. Soc. 123*, 11775−11781.
32. Abe, Y., and Krimm, S. (1972) Normal vibrations of polyglycine-II, *Biopolymers 11*, 1841−1853.
33. Abe, Y., and Krimm, S. (1972) Normal vibrations of crystalline polyglycine-I, *Biopolymers 11*, 1817−1839.
34. Dwivedi, A. M., and Krimm, S. (1982) Vibrational analysis of peptides, polypeptides, and proteins. XV. Crystalline polyglycine-II, *Biopolymers 21*, 2377−2397.
35. Moore, W. H., and Krimm, S. (1976) Vibrational analysis of peptides, polypeptides, and proteins. I. polyglycine I, *Biopolymers 15*, 2439−2464.
36. Snell, C. R., and Fasman, G. D. (1973) Kinetics and thermodynamics of α-helix D β transconformation of poly(L-lysine) and L-leucine copolymers. A compensation phenomenon, *Biochemistry 12*, 1017−1025.
37. Sugawara, Y., Harada, I., Matsuura, H., and Shimanouchi, T. (1978) Preresonance Raman studies of poly(L-lysine), poly(L-glutamic acid), and deuterated *N*-methylacetamides, *Biopolymers 17*, 1405−1421.
38. Yu, T. J., Lippert, J. L., and Peticola, Wl. (1973) Laser Raman studies of conformational variations of poly-L-lysine, *Biopolymers 12*, 2161−2176.
39. Kundu, A., and Kishore, N. (2004) Interaction of 2,2,2-trifluoroethanol with proteins: calorimetric, densimetric and surface tension approach, *Biophys. Chem. 109*, 427−442.
40. Luo, P. Z., and Baldwin, R. L. (1997) Mechanism of helix induction by trifluoroethanol: A framework for extrapolating the helix-forming properties of peptides from trifluoroethanol/water mixtures back to water, *Biochemistry 36*, 8413−8421.
41. Kentsis, A., and Sosnick, T. R. (1998) Trifluoroethanol promotes helix formation by destabilizing backbone exposure: Desolvation rather than native hydrogen bonding defines the kinetic pathway of dimeric coiled coil folding, *Biochemistry 37*, 14613−14622.
42. Jackson, M., Haris, P. I., and Chapman, D. (1989) Conformational transitions in poly(L-lysine): studies using Fourier transform infrared spectroscopy, *Biochim. Biophys. Acta 998*, 75−79.
43. Tu, A. T. (1986) Peptide backbone conformation and microenvironment of protein side-chains, in *Spectroscopy of Biological Systems* (Clark, R. J. H., and Hester, R. E., Eds.) pp 47−111, Wiley & Sons Ltd., New York.
44. Mikhonin, A. V., Myshakina, N. S., Bykov, S. V., and Asher, S. A. (2005) UV resonance Raman determination of polyproline II, extended 2.5_1-helix, and β-sheet ψ angle energy landscape in poly-L-lysine and poly-L-glutamic acid, *J. Am. Chem. Soc. 127*, 7712−7720.
45. Tiffany, M. L., and Krimm, S. (1968) Circular dichroism of poly-L-proline in an unordered conformation, *Biopolymers 6*, 1767−1770.
46. Measey, T., and Schweitzer-Stenner, R. (2005) Simulation of amide I′ band profiles of trans polyproline based on an excitonic coupling model, *Chem. Phys. Lett. 408*, 123−127.
47. Wooley, S. Y. C., and Holzwart, G. (1970) Intramolecular β-pleated-sheet formation by poly-L-lysine in solution, *Biochemistry 9*, 3604−3608.
48. Greenfield N., Davidson, B., and Fasman, G. D. (1967) Use of computed optical rotatory dispersion curves for evaluation of protein conformation, *Biochemistry 6*, 1630−1637.
49. Copeland, R. A., and Spiro, T. G. (1986) Ultraviolet Raman hypochromism of the tropomyosin amide modes: A new method for estimating α-helical content in proteins, *J. Am. Chem. Soc. 108*, 1281−1285.
50. Huang, C. Y., Klemke, J. W., Getahun, Z., DeGrado, W. F., and Gai, F. (2001) Temperature-dependent helix-coil transition of an alanine based peptide, *J. Am. Chem. Soc. 123*, 9235−9238.
51. Lednev, I. K., Karnoup, A. S., Sparrow, M. C., and Asher, S. A. (2001) Transient UV Raman spectroscopy finds no crossing barrier between the peptide α-helix and fully random coil conformation, *J. Am. Chem. Soc. 123*, 2388−2392.
52. Syme, C. D., Blanch, E. W., Holt, C., Jakes, R., Goedert, M., Hecht, L., and Barron, L. D. (2002) A Raman optical activity study of rheomorphism in caseins, synucleins and tau: New insight into the structure and behaviour of natively unfolded proteins, *Eur. J. Biochem. 269*, 148−156.
53. Jordan, T., and Spiro, T. G. (1995) UV resonance Raman spectroscopy of *cis*-amides, *J. Raman Spectrosc. 26*, 867−876.
54. Blondelle, S. E., Forood, B., Houghten, R. A., and Perez-Paya, E. (1997) Polyalanine-based peptides as models for self-associated β-pleated-sheet complexes, *Biochemistry 36*, 8393−8400.

BI051507V